OHGO, Y. & TAKEUCHI, S. (1985). *J. Chem. Soc. Chem. Commun.* pp. 21–23.
OHGO, Y., TAKEUCHI, S., NATORI, Y., YOSHIMURA, J., OHASHI, Y. & SASADA, Y. (1981). *Bull. Chem. Soc. Jpn*, **54**, 3095–3099.
SHELDRICK, G. M. (1976). *SHELX76*. Program for crystal structure determination. Univ. of Cambridge, England.
UCHIDA, A., DANNO, M., SASADA, Y. & OHASHI, Y. (1987). *Acta Cryst.* B**43**, 528–532.
UCHIDA, A., OHASHI, Y. & SASADA, Y. (1986). *Nature (London)*, **320**, 51–52.
UCHIDA, A., OHASHI, Y., SASADA, Y. & OHGO, Y. (1985). *Acta Cryst.* C**41**, 25–26.

*Acta Cryst.* (1988). B**44**, 254–259

# Electron Density in the Spin Crossover Complex *trans*-[*N*,*N*′-Ethylenebis(salicylideneaminato)]bis(imidazole)iron(III) Perchlorate

BY A. M. MILNE AND E. N. MASLEN

*Crystallography Centre, University of Western Australia, Nedlands, Western Australia* 6009, *Australia*

(*Received* 6 *April* 1987; *accepted* 3 *November* 1987)

## Abstract

The title compound, $[Fe(salen)(imd)_2]ClO_4$, $[Fe(C_{16}H_{14}N_2O_2)(C_3H_4N_2)_2]ClO_4$, has an orthorhombic structure, $P2_12_12_1$ with $Z=4$, $a=15{\cdot}411$ (7), $b=13{\cdot}328$ (7), $c=11{\cdot}149$ (4) Å at 120 K, and $a=15{\cdot}556$ (6), $b=13{\cdot}495$ (6), $c=11{\cdot}468$ (4) Å at 295 K, $\lambda(Mo\ K\alpha)=0{\cdot}71069$ Å, $M_r=557{\cdot}77$, $F(000)=287$. Over that temperature range the magnetic moment increases sharply from 2·1 to 5·5 Bohr magnetons. The Fe atom coordinates in a slightly distorted octahedron with four N and two O ligands. The plane of one imidazole group bisects two N—Fe—O angles. The other is approximately coplanar with Fe—N and Fe—O vectors. The average length of the Fe—N bonds increases by 0·16 Å during that transition. Atomic charges derived from the electron difference density indicate that roughly 0·5 electrons are transferred to the Fe/ligand system in the spin transition. The changes in the topography of the density from low to room temperature are related to the increases in bond lengths, but are inconsistent with a model for the electron density derived from 3*d* states alone. The maxima are tetrahedrally disposed, and oriented so as to reduce interaction with the ligating N and O atoms. The idealized form of the low-temperature difference density is consistent with that expected for *both* imidazole rings oriented in the bisecting position, and at right angles to each other. This would favour interaction between the lone-pair 3*d* electrons and four imidazole H atoms.

## Introduction

Changes in spin state induce marked changes in the structural geometries of crystalline materials. Reversible temperature-dependent spin transitions are favourable for study, because of the simple relationship between the structures of the low- and high-temperature forms. It may be difficult to characterize the states involved from structural geometry alone, and in principle measurement of the difference density by diffraction experiments should help in identifying the states involved in the transition. However, spin crossover complexes are labile because of their structural instability, and it is difficult to achieve the accuracy desired in the diffraction data.

The magnetic properties of the spin crossover complex $[Fe(salen)(imd)_2]ClO_4$ were determined by Kennedy, McGrath, Murray, Skelton & White (1987), who also determined crystal structures below (120 K) and above (295 K) the transition. The system is a useful model for studying spin equilibrium in heme proteins. The quality of the diffraction data indicated that, with care, the standards required for a charge density study of modest quality might be achieved.

Table 1. *Crystal data and refinement details*

| | 120 K | 295 K |
|---|---|---|
| $V$ (Å$^3$) | 2290 (2) | 2407 (2) |
| $D_x$ (Mg m$^{-3}$) | 1·617 | 1·538 |
| $\mu$ (mm$^{-1}$) | 0·826 | 0·786 |
| $N$ measured | 25572 | 17599 |
| $N$ unique | 7215 | 4866 |
| $h, k, l$ range | $0 \le h \le 27, 0 \le k \le 23,$ $0 \le l \le 19$ | $0 \le h \le 23, 0 \le k \le 20,$ $0 \le l \le 17$ |
| $(\sin\theta)/\lambda$ (Å$^{-1}$) | ≤0·883 | ≤0·856 |
| $R_{int}$ | 0·025 | 0·026 |
| $R$ | 0·071 | 0·074 |
| $wR$ | 0·042 | 0·042 |
| $S$ | 1·51 (1) | 2·14 (2) |
| $1/\sigma_{max}$ | 0·01 | 0·01 |

## Experimental

The data sets measured by Kennedy, McGrath, Murray, Skelton & White (1987) were scrutinized and carefully extended. Crystal irregularly shaped with $(10\bar{1})$, $(12\bar{1})$, $(011)$, $(101)$, $(1\bar{2}0)$, $(\bar{2}01)$, $(\bar{1}2\bar{1})$, $(02\bar{1})$ faces at distances of 0·11, 0·17, 0·10, 0·14, 0·148, 0·11, 0·10 and 0·30 mm respectively from a common centre. Data measured on a Syntex $P2_1$ diffractometer

0108-7681/88/030254-06$03.00

Table 2. *Fractional atomic coordinates and equivalent isotropic thermal parameters* (Å$^2$)

$$B_{eq} = 8\pi^2/3 \sum_i \sum_j U_{ij} a_i^* a_j^* \mathbf{a}_i.\mathbf{a}_j.$$

| | 120 K | | | | 295 K | | | |
|---|---|---|---|---|---|---|---|---|
| | $x$ | $y$ | $z$ | $B_{eq}$ | $x$ | $y$ | $z$ | $B_{eq}$ |
| Fe(1) | 0·19189 (3) | 0·85796 (3) | 0·84465 (3) | 0·80 | 0·19913 (3) | 0·86561 (3) | 0·84094 (4) | 2·62 |
| O(11) | 0·3026 (1) | 0·9039 (1) | 0·7983 (2) | 1·16 | 0·3135 (1) | 0·8924 (2) | 0·7962 (2) | 3·69 |
| C(11) | 0·3722 (2) | 0·8484 (2) | 0·7979 (2) | 1·09 | 0·3799 (2) | 0·8309 (3) | 0·7974 (3) | 3·69 |
| C(16) | 0·3718 (2) | 0·7415 (2) | 0·7932 (3) | 1·16 | 0·3707 (2) | 0·7275 (3) | 0·7885 (3) | 3·86 |
| C(15) | 0·4512 (2) | 0·6888 (2) | 0·7916 (3) | 1·62 | 0·4462 (3) | 0·6682 (4) | 0·7892 (4) | 5·84 |
| C(14) | 0·5292 (2) | 0·7370 (3) | 0·7968 (3) | 1·77 | 0·5261 (3) | 0·7114 (6) | 0·7977 (4) | 7·30 |
| C(13) | 0·5307 (2) | 0·8432 (3) | 0·7996 (3) | 1·85 | 0·5344 (3) | 0·8108 (6) | 0·8062 (4) | 7·85 |
| C(12) | 0·4543 (2) | 0·8964 (2) | 0·7980 (3) | 1·42 | 0·4637 (3) | 0·8720 (4) | 0·8040 (3) | 5·27 |
| C(17) | 0·2921 (2) | 0·6850 (2) | 0·7851 (2) | 1·20 | 0·2893 (3) | 0·6778 (3) | 0·7803 (3) | 3·64 |
| N(18) | 0·2169 (1) | 0·7228 (2) | 0·8024 (2) | 1·02 | 0·2162 (2) | 0·7199 (2) | 0·7962 (2) | 3·02 |
| C(19) | 0·1375 (2) | 0·6646 (2) | 0·7814 (3) | 1·30 | 0·1344 (3) | 0·6677 (2) | 0·7766 (3) | 3·80 |
| O(21) | 0·1638 (1) | 0·9946 (1) | 0·8832 (2) | 1·02 | 0·1601 (1) | 0·9963 (2) | 0·8801 (2) | 2·99 |
| C(21) | 0·0883 (2) | 1·0268 (2) | 0·9236 (2) | 1·01 | 0·0854 (2) | 1·0265 (2) | 0·9220 (3) | 2·82 |
| C(26) | 0·0143 (2) | 0·9649 (2) | 0·9430 (2) | 1·14 | 0·0128 (2) | 0·9649 (3) | 0·9390 (3) | 3·19 |
| C(25) | −0·0632 (2) | 1·0092 (2) | 0·9854 (3) | 1·44 | −0·0619 (2) | 1·0058 (3) | 0·9841 (3) | 3·95 |
| C(24) | −0·0688 (2) | 1·1090 (3) | 1·0107 (3) | 1·66 | −0·0693 (3) | 1·1036 (3) | 1·0123 (4) | 4·64 |
| C(23) | 0·0040 (2) | 1·1691 (2) | 0·9921 (3) | 1·43 | 0·0026 (3) | 1·1633 (3) | 0·9969 (3) | 4·54 |
| C(22) | 0·0806 (2) | 1·1309 (2) | 0·9500 (2) | 1·21 | 0·0774 (2) | 1·1269 (3) | 0·9533 (3) | 3·33 |
| C(27) | 0·0141 (2) | 0·8584 (2) | 0·9231 (2) | 1·21 | 0·0140 (2) | 0·8575 (3) | 0·9174 (3) | 3·40 |
| N(28) | 0·0797 (2) | 0·8068 (2) | 0·8864 (2) | 1·08 | 0·0782 (2) | 0·8081 (2) | 0·8827 (2) | 2·96 |
| C(29) | 0·0726 (2) | 0·6962 (2) | 0·8769 (3) | 1·44 | 0·0713 (2) | 0·7001 (3) | 0·8703 (4) | 4·11 |
| N(31) | 0·1487 (2) | 0·8829 (2) | 0·6796 (2) | 0·97 | 0·1531 (2) | 0·8867 (2) | 0·6666 (2) | 2·87 |
| C(32) | 0·0762 (2) | 0·9281 (2) | 0·6489 (3) | 1·23 | 0·0806 (2) | 0·9291 (3) | 0·6379 (3) | 3·76 |
| N(33) | 0·0680 (2) | 0·9303 (2) | 0·5284 (2) | 1·46 | 0·0705 (2) | 0·9270 (3) | 0·5217 (3) | 4·53 |
| C(34) | 0·1394 (2) | 0·8829 (2) | 0·4805 (3) | 1·49 | 0·1389 (3) | 0·8803 (4) | 0·4764 (3) | 5·01 |
| C(35) | 0·1885 (2) | 0·8539 (2) | 0·5737 (2) | 1·20 | 0·1899 (2) | 0·8542 (3) | 0·5655 (3) | 3·66 |
| N(41) | 0·2326 (1) | 0·8366 (2) | 1·0124 (2) | 0·94 | 0·2358 (2) | 0·8361 (2) | 1·0182 (3) | 3·28 |
| C(42) | 0·2433 (2) | 0·9104 (2) | 1·0903 (3) | 1·33 | 0·2460 (2) | 0·9064 (3) | 1·0952 (3) | 3·81 |
| N(43) | 0·2722 (2) | 0·8765 (2) | 1·1967 (2) | 1·27 | 0·2755 (2) | 0·8710 (2) | 0·1968 (3) | 3·95 |
| C(44) | 0·2818 (2) | 0·7740 (2) | 1·1865 (3) | 1·56 | 0·2860 (3) | 0·7703 (3) | 1·1833 (3) | 4·34 |
| C(45) | 0·2568 (2) | 0·7496 (2) | 1·0722 (3) | 1·42 | 0·2614 (3) | 0·7501 (3) | 1·0717 (3) | 3·89 |
| Cl(1) | 0·16765 (4) | 0·43137 (5) | 0·97066 (7) | 1·29 | 0·16618 (6) | 0·43325 (7) | 0·9660 (1) | 4·23 |
| O(1) | 0·1227 (2) | 0·4174 (2) | 0·8586 (2) | 1·93 | 0·1218 (2) | 0·4187 (3) | 0·8583 (3) | 6·66 |
| O(2) | 0·2098 (2) | 0·3404 (2) | 1·0051 (3) | 2·61 | 0·2015 (3) | 0·3446 (2) | 1·0055 (3) | 8·42 |
| O(3) | 0·2311 (1) | 0·5099 (2) | 0·9584 (2) | 2·29 | 0·2312 (2) | 0·5054 (3) | 0·9539 (4) | 8·10 |
| O(4) | 0·1053 (2) | 0·4599 (2) | 1·0615 (2) | 2·48 | 0·1040 (2) | 0·4700 (3) | 1·0474 (3) | 7·97 |
| H(15) | 0·449 (2) | 0·613 (2) | 0·783 (3) | 0·56 | 0·436 (2) | 0·600 (3) | 0·780 (3) | 6·10 |
| H(14) | 0·580 (2) | 0·704 (2) | 0·803 (3) | 1·51 | 0·584 (2) | 0·677 (3) | 0·808 (3) | 5·49 |
| H(13) | 0·586 (2) | 0·881 (2) | 0·795 (3) | 1·23 | 0·588 (3) | 0·841 (3) | 0·797 (4) | 8·30 |
| H(12) | 0·456 (2) | 0·971 (2) | 0·795 (3) | 1·84 | 0·454 (3) | 0·948 (3) | 0·805 (4) | 8·68 |
| H(17) | 0·300 (2) | 0·617 (2) | 0·772 (3) | 0·19 | 0·285 (2) | 0·607 (2) | 0·764 (2) | 2·19 |
| H(19*a*) | 0·115 (2) | 0·681 (2) | 0·703 (3) | 0·89 | 0·116 (2) | 0·683 (2) | 0·707 (3) | 3·96 |
| H(19*b*) | 0·143 (3) | 0·598 (3) | 0·765 (4) | 2·68 | 0·140 (2) | 0·594 (2) | 0·773 (3) | 4·30 |
| H(25) | −0·112 (2) | 0·963 (2) | 0·986 (3) | 1·03 | −0·101 (2) | 0·977 (2) | 0·976 (3) | 4·21 |
| H(24) | −0·124 (2) | 1·143 (2) | 1·042 (3) | 0·81 | −0·116 (2) | 1·135 (2) | 1·048 (3) | 3·51 |
| H(23) | 0·003 (3) | 1·236 (3) | 1·006 (4) | 3·59 | 0·004 (2) | 1·228 (2) | 1·013 (3) | 3·80 |
| H(22) | 0·125 (2) | 1·167 (2) | 0·930 (3) | 1·16 | 0·120 (2) | 1·166 (2) | 0·936 (3) | 3·32 |
| H(27) | −0·045 (2) | 0·829 (2) | 0·940 (2) | −0·30 | −0·037 (2) | 0·828 (2) | 0·922 (2) | 2·38 |
| H(29*a*) | 0·093 (2) | 0·664 (2) | 0·951 (2) | −0·10 | 0·090 (2) | 0·672 (2) | 0·951 (2) | 1·37 |
| H(29*b*) | 0·016 (2) | 0·678 (2) | 0·842 (3) | 1·30 | 0·008 (2) | 0·681 (2) | 0·837 (3) | 3·84 |
| H(32) | 0·031 (2) | 0·945 (2) | 0·698 (3) | 1·08 | 0·038 (2) | 0·948 (2) | 0·697 (3) | 3·42 |
| H(33) | 0·024 (3) | 0·962 (3) | 0·500 (5) | 6·59 | 0·022 (2) | 0·948 (3) | 0·476 (3) | 5·40 |
| H(34) | 0·145 (2) | 0·882 (2) | 0·402 (3) | 0·50 | 0·147 (2) | 0·864 (2) | 0·407 (2) | 2·31 |
| H(35) | 0·246 (2) | 0·824 (2) | 0·568 (2) | −0·22 | 0·244 (2) | 0·817 (2) | 0·563 (3) | 3·81 |
| H(42) | 0·227 (3) | 0·975 (3) | 1·077 (3) | 3·46 | 0·222 (1) | 0·979 (2) | 1·091 (2) | 2·47 |
| H(43) | 0·285 (3) | 0·912 (3) | 1·263 (4) | 3·33 | 0·291 (2) | 0·900 (3) | 1·261 (3) | 5·03 |
| H(44) | 0·305 (3) | 0·735 (3) | 1·256 (4) | 3·23 | 0·309 (2) | 0·732 (3) | 1·247 (3) | 5·33 |
| H(45) | 0·251 (2) | 0·683 (2) | 1·036 (3) | 0·39 | 0·255 (2) | 0·692 (2) | 1·040 (2) | 1·83 |

in $\omega$–$2\theta$ mode. The intensities of the standard 800, $\bar{8}00$, 040, $0\bar{4}0$ and 004 reflections monitored after every hundred ordinary reflections. For the low-temperature structure the variations were proportional to each other, and consistent with fluctuations of the primary-beam intensity over a $\pm 10\%$ range. For the room-temperature data collection, the range of variation initially was similar, but in the later stage the changes became inconsistent, indicating chemical decomposition of the sample. Data collection was terminated, so the data set has less redundancy than that for the low-temperature structure. Other details are given, with those of the structure refinement, in Table 1. *XTAL* (Stewart & Hall, 1983) programs were used for all calculations, on a Perkin–Elmer 3240 computer. Scattering factors for bonded H atoms by Stewart, Davidson & Simpson (1965), and the free-atom values and dispersion corrections for Fe, Cl, C, N, O from *International Tables for X-ray Crystallography* (1974). Data corrected for absorption analytically using the program *ABSORB*. Absorption-factor range 0·83–0·87. Structures refined using residuals based on $|F|$ with the program *SFSLX*, weights $w = 1/\sigma^2(F)$. For the low-temperature structure, three of the H atoms had small non-positive-definite temperature factors. Extinction was negligible.

Table 3. *Bond lengths not involving* H *atoms* (Å)

| | 120 K | 295 K | | 120 K | 295 K |
|---|---|---|---|---|---|
| O(11)–C(11) | 1·302 (3) | 1·326 (4) | O(21)–C(21) | 1·320 (3) | 1·322 (4) |
| C(11)–C(12) | 1·418 (4) | 1·418 (6) | C(21)–C(22) | 1·422 (4) | 1·407 (5) |
| C(12)–C(13) | 1·374 (4) | 1·376 (8) | C(22)–C(23) | 1·368 (4) | 1·359 (6) |
| C(13)–C(14) | 1·417 (5) | 1·350 (11) | C(23)–C(24) | 1·394 (4) | 1·391 (6) |
| C(14)–C(15) | 1·365 (5) | 1·379 (7) | C(24)–C(25) | 1·364 (4) | 1·365 (6) |
| C(15)–C(16) | 1·411 (4) | 1·420 (6) | C(25)–C(26) | 1·413 (4) | 1·386 (5) |
| C(16)–C(11) | 1·427 (4) | 1·407 (6) | C(26)–C(21) | 1·424 (4) | 1·416 (5) |
| N(31)–C(32) | 1·316 (4) | 1·307 (4) | N(41)–C(42) | 1·321 (4) | 1·305 (5) |
| C(32)–N(33) | 1·350 (4) | 1·342 (5) | C(42)–N(43) | 1·345 (4) | 1·340 (5) |
| N(33)–C(34) | 1·376 (4) | 1·342 (5) | N(43)–C(44) | 1·378 (4) | 1·377 (5) |
| C(34)–C(35) | 1·343 (4) | 1·341 (5) | C(44)–C(45) | 1·370 (4) | 1·365 (5) |
| C(35)–N(31) | 1·386 (3) | 1·366 (4) | C(45)–N(41) | 1·390 (4) | 1·371 (5) |
| Fe–O(11) | 1·884 (2) | 1·886 (2) | C(16)–C(17) | 1·444 (4) | 1·436 (6) |
| Fe–N(18) | 1·902 (2) | 2·050 (3) | C(26)–C(27) | 1·436 (4) | 1·470 (5) |
| Fe–O(21) | 1·921 (2) | 1·918 (2) | C(17)–N(18) | 1·278 (4) | 1·285 (5) |
| Fe–N(28) | 1·916 (2) | 2·091 (3) | C(27)–N(28) | 1·290 (4) | 1·264 (4) |
| Fe–N(31) | 1·985 (2) | 2·142 (3) | N(18)–C(19) | 1·468 (4) | 1·470 (5) |
| Fe–N(41) | 1·993 (2) | 2·149 (3) | N(28)–C(29) | 1·484 (4) | 1·469 (4) |
| | | | C(19)–C(29) | 1·520 (4) | 1·519 (6) |
| Cl–O(1) | 1·441 (3) | 1·429 (4) | | | |
| Cl–O(2) | 1·427 (3) | 1·392 (3) | | | |
| Cl–O(3) | 1·439 (2) | 1·411 (4) | | | |
| Cl–O(4) | 1·446 (3) | 1·433 (4) | | | |

Atomic coordinates are given in Table 2.* Selected bond lengths and angles are listed in Table 3. *ORTEP* diagrams (Johnson, 1965) are shown in Fig. 1. In both structures the imidazole ring containing N(41) is approximately coplanar with the Fe–N(18) and Fe–O(21) bonds, whereas that containing N(31) bisects the N(18)–Fe–O(11) and N(28)–Fe–O(21) angles.

The bond lengths in Table 2 show large extensions of 0·148 (4), 0·156 (4), 0·157 (4) and 0·175 (4) Å for Fe–N(18), Fe–N(41), Fe–N(31) and Fe–N(28) respectively due to the spin transition. The corresponding changes of 0·002 (3) and −0·002 (3) Å for the Fe–O(11) and Fe–O(21) bonds are small.

## Electron density

Difference densities for both low- and room-temperature structures were evaluated. Sections containing the Fe atom and the nearest neighbours, including the imidazole N atoms, are shown in Fig. 2. In the low-spin form the density along the Fe–O bonds is strongly depleted. Overlap of the electron pairs in the electron-rich O atom and the paired spins in the Fe atom's 3*d* subshell reduces the electron density in the region of overlap owing to exchange. Positive density tends to accumulate near the Fe atom between the ligands, and there are some indications of lone-pair development near the N atoms. However, there is little consistency from one Fe–N bond to another. As shown in Fig. 2(*a*), the electron density concentrates in the N(28)–Fe–N(41) angle, maximizing close to the Fe–N(28) bond, whereas there is a marked electron deficiency in the N(18)–Fe–N(41) angle, as shown in Fig. 2(*b*).

There is a limited degree of correspondence between the topography of the difference density and nearest-neighbour geometry, restricted to a subgroup of the symmetry. One's first instict is to conclude that the map is predominantly due to experimental noise. However, more careful examination of Fig. 2(*a*) shows fairly strong 3*m* pseudosymmetry in addition to the coincidence of one approximate mirror plane with that in the molecular geometry. The corresponding map for the high-temperature form, Fig. 2(*c*), has similar symmetry, based on axes with the same orientation.

There are further similarities between the maps with lower symmetry. In Figs. 2(*b*) and 2(*d*), the density along the Fe–O(21) bond and in the N(18)–Fe–N(41) angle is depleted, while along Fe–N(31) it is enhanced, with the maximum displaced slightly towards the O(21) atom in both cases.

The consistency was checked by evaluating atomic charges by the method of Hirshfeld (1977), which are listed in Table 4. The charges for first-row atoms with low thermal motion which are little affected by the spin transition agree closely. The correlation coefficient

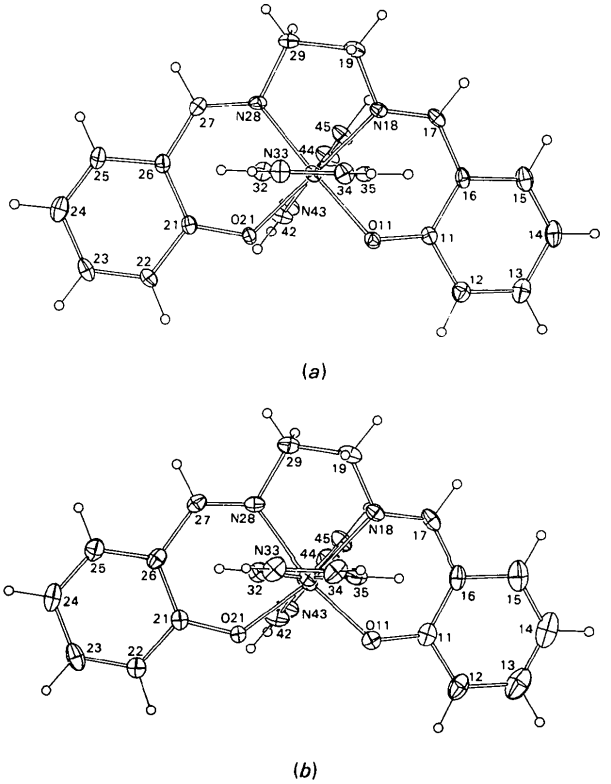


Fig. 1. Molecular structure of $[Fe(salen)(imd)_2]ClO_4$. (*a*) At 120 K, 50% probability ellipsoids. (*b*) At 295 K, 20% probability ellipsoids.

* Lists of structural parameters, bond lengths and angles, thermal parameters and structure factors have been deposited with the British Library Document Supply Centre as Supplementary Publication No. SUP 44480 (57 pp.). Copies may be obtained through The Executive Secretary, International Union of Crystallography, 5 Abbey Square, Chester CH1 2HU, England.

$\sum Q_{120}Q_{295}(\sum Q_{120}^2 \sum Q_{295}^2)^{-1/2}$ between the charges $Q$ in the two structures is 0·74 for 58 values, which is highly significant.

Associated with the spin transition is an increase of 0·52 electrons in the electron count on the central moiety, *i.e.* on the Fe atom and its nearest neighbours N(18), N(28), N(31), N(41), O(11) and O(21). This increase is expected because of reduced exchange depletion of the electron density along the Fe–N bonds as those bonds expand.

The charges on the perchlorate groups are −0·66 and −0·44 for the low- and room-temperature structures respectively. These are similar to values reported for complex ions in other structures. For the room-temperature structure the charges on the perchlorate O atoms are less consistent than those at low temperature – a result which is not unexpected because of increased thermal motion. However, other analyses (Maslen, Ridout & Watson, 1988) indicate that group charges are determined more accurately than predicted from a simple accumulation of errors in such cases.

The difference density maxima for the high-spin form shown in Fig. 2(*c*) extend approximately 1 Å along a ring centred on the Fe atom. As shown in Fig. 2(*c*), the directions of the extensions for the three maxima related by $3m$ symmetry correspond to rotation about the threefold axis. The atoms of the N(41) imidazole groups librate strongly about that axis in the room-temperature structure. The extended nature of the peaks in Fig. 2(*c*) could be expected if they are related to the imidazole groups.

The differences between the low- and room-temperature cases are consistent with the structural changes, noting what is expected for a spin transition. The three maxima surrounding the Fe site in Fig. 2(*a*) are roughly 0·5 Å from the nuclear position, whereas the corresponding peaks in Fig. 2(*c*) are about 0·8 Å from that site. This represents an expansion of the $t_{2g}$ maxima similar to that reported for cobalt complexes by Maslen & Ridout (1987).

This displacement of the electrons with parallel spins away from the metal nucleus is accompanied by, and at least partly responsible for, the increase in the Fe–N bond lengths. However, the change in spin state also has the effect of reducing the depletion of the electron density along the Fe–O bonds, close to the Fe nucleus.

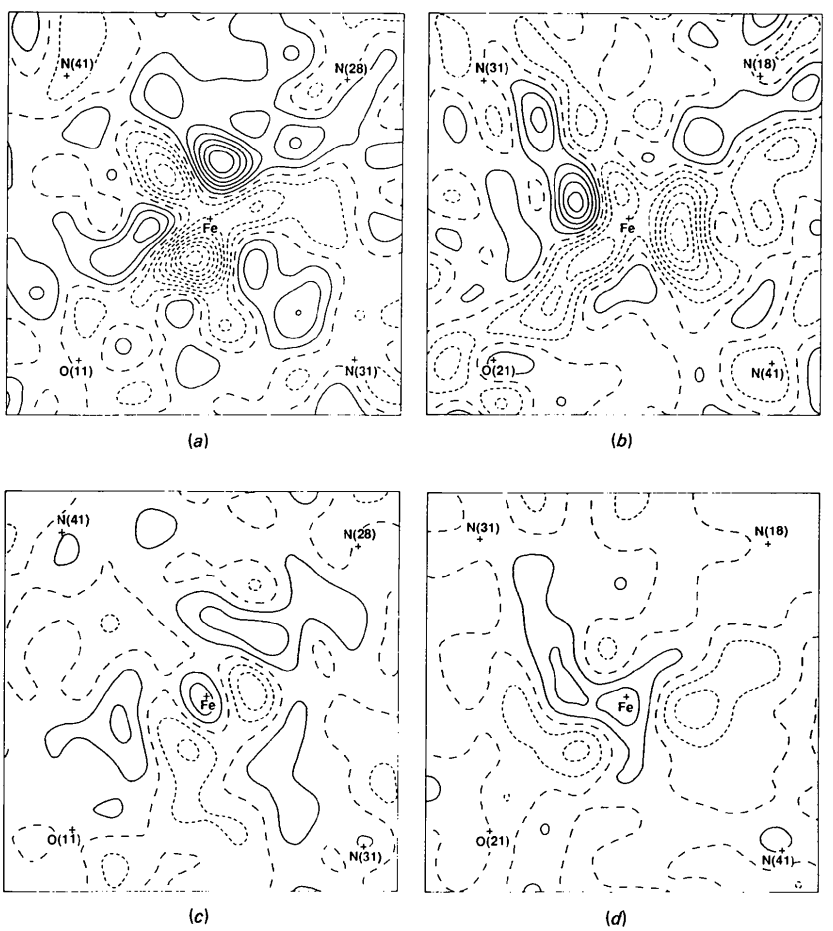


Fig. 2. Difference density for [Fe(salen)-(imd)$_2$]ClO$_4$. (*a*) Plane containing Fe, N(31), O(11), N(41), N(28) at 120 K. (*b*) Plane containing Fe, N(31), O(21), N(41), N(18) at 120 K. (*c*) Plane containing Fe, N(31), O(11), N(41), N(28) at 295 K. (*d*) Plane containing Fe, N(31), O(21), N(41), N(18) at 295 K. Contour interval 0·2 e Å$^{-3}$. Zero contour broken, negative contours dotted.

Table 4. *Atomic charges in electrons*

Standard deviations calculated by the method of Davis & Maslen (1978).

| | 120 K | 295 K | | 120 K | 295 K |
|---|---|---|---|---|---|
| Fe | 0·06 (4) | −0·08 (2) | C(27) | 0·06 (4) | −0·04 (2) |
| O(11) | −0·20 (4) | −0·22 (2) | H(27) | 0·07 (4) | −0·06 (2) |
| C(11) | −0·13 (4) | −0·11 (2) | N(28) | −0·24 (4) | −0·16 (2) |
| C(12) | 0·04 (4) | −0·02 (2) | C(29) | −0·07 (4) | 0·06 (2) |
| H(12) | 0·02 (4) | 0·05 (2) | H(29a) | 0·10 (4) | 0·20 (2) |
| C(13) | 0·07 (4) | 0·04 (2) | H(29b) | −0·01 (4) | 0·08 (2) |
| H(13) | 0·00 (4) | 0·07 (2) | N(31) | 0·12 (4) | −0·01 (2) |
| C(14) | −0·16 (4) | −0·12 (2) | C(32) | 0·15 (4) | 0·09 (2) |
| H(14) | −0·15 (4) | −0·14 (2) | H(32) | −0·03 (4) | 0·02 (2) |
| C(15) | 0·00 (4) | −0·01 (2) | N(33) | −0·05 (4) | −0·06 (2) |
| H(15) | 0·01 (4) | 0·11 (2) | H(33) | 0·03 (4) | 0·05 (2) |
| C(16) | −0·08 (4) | −0·23 (2) | C(34) | 0·10 (4) | −0·03 (2) |
| C(17) | 0·09 (4) | −0·05 (2) | H(34) | 0·05 (4) | 0·03 (2) |
| H(17) | 0·03 (4) | 0·02 (2) | C(35) | 0·17 (4) | 0·13 (2) |
| N(18) | −0·00 (4) | −0·02 (2) | H(35) | 0·05 (4) | 0·05 (2) |
| C(19) | 0·11 (4) | 0·06 (2) | N(41) | −0·10 (4) | −0·18 (2) |
| H(19a) | 0·06 (4) | 0·07 (2) | C(42) | −0·15 (4) | −0·05 (2) |
| H(19b) | 0·05 (4) | 0·07 (2) | H(42) | 0·02 (4) | 0·11 (2) |
| O(21) | 0·11 (4) | 0·00 (2) | N(43) | 0·03 (4) | 0·07 (2) |
| C(21) | 0·18 (4) | 0·11 (2) | H(43) | 0·15 (4) | 0·20 (2) |
| C(22) | 0·09 (4) | 0·27 (2) | C(44) | −0·13 (4) | −0·11 (2) |
| H(22) | 0·04 (4) | 0·11 (2) | H(44) | 0·01 (4) | 0·09 (2) |
| C(23) | 0·07 (4) | 0·17 (2) | C(45) | 0·11 (4) | 0·09 (2) |
| H(23) | 0·06 (4) | 0·09 (2) | H(45) | 0·21 (4) | 0·22 (2) |
| C(24) | −0·07 (4) | −0·05 (2) | Cl | 0·06 (4) | −0·04 (2) |
| H(24) | −0·06 (4) | 0·00 (2) | O(1) | −0·25 (4) | −0·28 (2) |
| C(25) | −0·08 (4) | −0·06 (2) | O(2) | −0·34 (4) | −0·10 (2) |
| H(25) | −0·05 (4) | −0·03 (2) | O(3) | −0·13 (4) | −0·15 (2) |
| C(26) | −0·12 (4) | −0·10 (2) | O(4) | −0·00 (4) | 0·13 (2) |

This must lower the exchange repulsion between the Fe and O atoms, counterbalancing the extra repulsion due to the increase in spin for the Fe 3*d* electrons. The two effects cancel, so that the Fe–O bond lengths remain unchanged.

For the Fe–N bonds, on the other hand, there is no pronounced depletion of the electron density near the Fe nucleus in the low-temperature form. Along the Fe–N(28) bond the spin transition reduces the electron density strongly, which is expected to lengthen that bond. The spin transition lengthening is especially large for that Fe–N bond. The differences between the expansions for the other three Fe–N bonds is of limited significance. Although not obvious from the sections shown in Fig. 2, the maximum concentrations of electron density near these three bonds are similar.

Encouraged by this consistency, we mapped the disposition of the principal features in the low-temperature difference density in three dimensions. There are sets of four peaks with maximum magnitude 1·2 e Å$^{-3}$, and four related hollows, tetrahedrally disposed and lying on the vertices of a cube approximately 0·5 Å from the Fe site. In contrast with the diffuse maxima for the high-temperature form, the difference density maxima for the low-temperature form are compact, as expected for the lone pairs in a low-spin system.

The difference density around the Fe atom is tetrahedral, close to antisymmetric, and is a reasonable approximation to $\bar{4}3m$ ($T_d$) symmetry. This is not fully consistent with the octahedral $m3m$ ($O_h$) symmetry for the ideal coordination, which applies if the bonds from the Fe to the N and O ligands are equivalent. Likewise, it is consistent neither with a simple theory of spin transitions based on repopulation of 3*d* states, nor with other theories based on combining 3*d* and 4*s* states only. Any linear combination of these states is symmetric, and cannot generate an antisymmetric density function.

To account for the change in symmetry we must identify a tetrahedral component in the perturbing field. The most obvious reduction in symmetry is due to non-equivalence of the ligating N(18) and N(28) atoms to the O(11) and O(21) atoms. However, the orientation of the features in the deformation density is not correlated with that asymmetry.

A careful examination was made of all interaction vectors, including those with the anions. There is no aspect of the structural geometry which correlates completely with the deformation density, but there is an

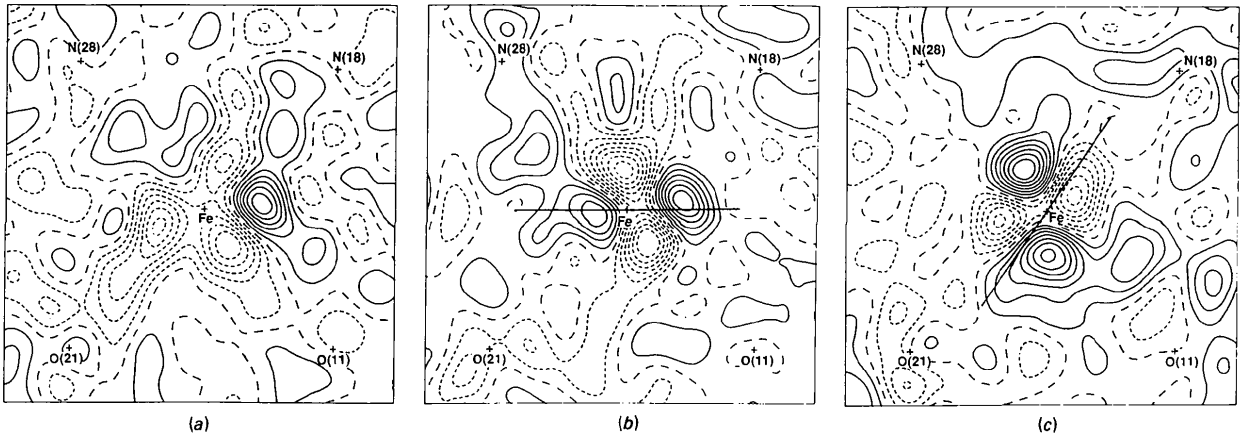


Fig. 3. Difference density for $[Fe(salen)(imd)_2]ClO_4$. (*a*) Equatorial plane containing Fe,O(11),N(18),N(28),O(21). (*b*) Plane 0·3 Å above (*a*), showing the projection of the plane of the N(31) imidazole group. (*c*) Plane 0·3 Å below (*a*), showing the projection of the plane of the N(41) imidazole group. Contours as for Fig. 2.

interesting relationship indicated in Fig. 3. Fig. 3(*a*) is a section through the equatorial plane containing Fe, N(18) and O(11), which also passes close to N(28) and O(21). Figs. 3(*b*) and 3(*c*) are sections parallel to Fig. 3(*a*), but 0·3 Å closer to the imidazole groups containing N(31) and N(41) respectively. It is clear from Fig. 3(*b*) that two of the tetrahedral maxima around the Fe atom are close to the plane containing the N(31) imidazole group, even though one of the maxima does not reach full height in the section shown. Both maxima are close to vectors linking the central Fe atom to imidazole H atoms.

As seen in Fig. 3(*c*), the deformation density is not symmetry related to the imidazole group containing N(41). To bring that subsystem into conformity with the arrangement in Fig. 3(*b*) would require rotation of the N(41) imidazole group by approximately 50° about the N(31)···N(41) vector. At that stage it would be at right angles to the N(31) imidazole group. In its actual configuration without that rotation, the N(41) imidazole has the configuration characteristic of the high-spin form of the cation, as identified in $[Fe(salen)(imd)_2]PF_6$ by Kennedy, McGrath, Murray, Skelton & White (1987).

We postulate that in the ideal low-spin structure the imidazole rings are at right angles to each other, and coincident with the planes bisecting the O(11)–Fe–N(18) and the N(18)–Fe–N(28) angles respectively. The vectors from the Fe to the four imidazole H atoms would then describe a tetrahedron similar to that defined by the lobes of excess density in the spin crossover complex shown in Fig. 3. However, only one imidazole group is actually in the configuration which favours low spin. The other is oriented so as to favour high spin, which is the reason for the instability in this structure. It is clear from packing diagrams (not shown) that the imidazole groups are held in this mixed configuration by solvent molecules – accounting for their effect on the spin transition. This explains the indirect nature of their role in the magnetic properties of the structures containing these complexes noted by Kennedy, McGrath, Murray, Skelton & White (1987).

Thanks are due to A. H. White, who suggested the problem, for supervising the data collection. This work was supported by the Australian Research Grants Scheme.

### References

DAVIS, C. L. & MASLEN, E. N. (1978). *Acta Cryst.* A**34**, 743–746.
*International Tables for X-ray Crystallography* (1974). Vol. IV. Birmingham: Kynoch Press. (Present distributor D. Reidel, Dordrecht.)
HIRSHFELD, F. L. (1977). *Theor. Chim. Acta*, **44**, 129–138.
JOHNSON, C. K. (1965). *ORTEP*. Report ORNL-3794. Oak Ridge National Laboratory, Tennessee, USA.
KENNEDY, B. J., MCGRATH, A. C., MURRAY, K. S., SKELTON, B. S. & WHITE, A. H. (1987). *Inorg. Chem.* **26**, 483–495.
MASLEN, E. N. & RIDOUT, S. C. (1987). *Acta Cryst.* B**43**, 352–356.
MASLEN, E. N., RIDOUT, S. C. & WATSON, K. J. (1988). *Acta Cryst.* B**44**, 96–101.
STEWART, J. M. & HALL, S. R. (1983). *XTAL User's Manual*. Computer Science Center, Univ. of Maryland, College Park, Maryland, USA.
STEWART, R. F., DAVIDSON, E. R. & SIMPSON, W. T. (1965). *J. Chem. Phys.* **42**, 3175–3187.

*Acta Cryst.* (1988). B**44**, 259–262

# Lattice-Energy Calculations on Organometallic Compounds

BY J. SANZ-APARICIO, S. MARTÍNEZ-CARRERA AND S. GARCÍA-BLANCO

*UEI de Cristalografia, Instituto 'Rocasolano', CSIC, Serrano* 119, 28006 *Madrid, Spain*

AND A. CONDE

*Departamento de Fisica del Estado Sólido, Instituto de CC de los Materiales de Sevilla, Universidad de Sevilla, CSIC,* 41080 *Sevilla, Spain*

(*Received* 5 *October* 1987; *accepted* 21 *January* 1988)

## Abstract

Lattice-energy calculations in the atom–atom approach have been performed for five organometallic compounds of previously determined crystal structure. Minimization of energy in terms of positional, orientational, torsional and cell parameters gave satisfactory results. Computation of energy as a function of torsion angle gave two-dimensional cross sections which present minimum-energy conformations at maximum deviations of 10° from the experimental conformations.

## Introduction

Packing analysis following the atom–atom approach (Kitaigorodsky, 1973) has been used in determining the crystal structure of a large variety of organic com-

0108-7681/88/030259-04$03.00